

Stationary-phase analysis of time-shift extended imaging in a constant-velocity model

Mulder, W. A.

DOI

[10.1111/1365-2478.13496](https://doi.org/10.1111/1365-2478.13496)

Publication date

2024

Document Version

Final published version

Published in

Geophysical Prospecting

Citation (APA)

Mulder, W. A. (2024). Stationary-phase analysis of time-shift extended imaging in a constant-velocity model. *Geophysical Prospecting*, 72(5), 1555-1563. <https://doi.org/10.1111/1365-2478.13496>

Important note

To cite this publication, please use the final published version (if applicable). Please check the document version above.

Copyright

Other than for strictly personal use, it is not permitted to download, forward or distribute the text or part of it, without the consent of the author(s) and/or copyright holder(s), unless the work is under an open content license such as Creative Commons.

Takedown policy

Please contact us and provide details if you believe this document breaches copyrights. We will remove access to the work immediately and investigate your claim.

Stationary-phase analysis of time-shift extended imaging in a constant-velocity model

W. A. Mulder^{1,2} 

¹Shell Global Solutions International B.V.,
Den Haag, The Netherlands

²Department of Geoscience & Engineering,
Faculty of Civil Engineering and
Geosciences, Delft University of
Technology, Delft, The Netherlands

Correspondence

W.A. Mulder, Shell Global Solutions
International B.V., Carel van Bylandtlaan
16, 2596 HR Den Haag, The Netherlands.
Email: Wim.Mulder@shell.com

Abstract

To estimate the depth errors in a subsurface model obtained from the inversion of seismic data, the stationary-phase approximation in a two-dimensional constant-velocity model with a dipped reflector is applied to migration with a time-shift extension. This produces two asymptotic solutions: one is a straight line, and the other is a curve. If the velocity differs from the true one, a closed-form expression of the depth error follows from the depth and apparent dip of the reflector as well as the position of the amplitude peak at a non-zero time shift, where the two solutions meet and the extended migration image focuses. The results are compared to finite-frequency results from a finite-difference code. A two-dimensional synthetic example with a salt diapir illustrates how depth errors can be estimated in an inhomogeneous model after inverting the seismic data for the velocity model.

KEYWORDS

computing aspects, inverse problem, mathematical formulation, seismics, wave

INTRODUCTION

Seismic data provide a subsurface model or image after solving an inverse problem (e.g., Schuster, 2017), often through some form of minimization or optimization at a considerable computational cost. Given the ill-posed character of the procedure, uncertainty quantification of the model parameters is the next step. In the classic approach (Backus & Gilbert, 1970; Tarantola, 2005), the forward modelling operator that simulates data given a model is linearized around the optimum of some cost function that describes how well the modelled data match the observations. The first derivative of the cost function with respect to the model parameters vanishes at the optimum, and the second derivative or Hessian approximately describes the uncertainty. In a typical full-waveform inversion (FWI) problem, the Hessian is too big to be computed, but estimates on sparser (Rickett, 2003) or coarser (Mulder & Kuvshinov, 2023) grids may suffice.

A disadvantage of this approach, in contrast to travel-time tomography, is that depth errors are not explicitly available but only implicitly through velocity errors. The purpose of the current paper is to estimate the local depth error of a P-wave velocity model, constructed by FWI or migration velocity analysis or another method. The main tool is based on an explicit expression, derived here, for the depth error in a time-shift extended migration image, given a constant velocity.

Migration refers to a class of methods that map seismic data to reflectors. In its original form, it requires selecting a subset of the data, known as primaries, which are waves that have travelled from the source to the reflector and back to the receivers without being reflected or scattered multiple times. The Green functions, which describe wave propagation in a subsurface model from one point to another, can be computed with a variety of methods. These range from simple travel times and amplitudes in a constant velocity model

This is an open access article under the terms of the Creative Commons Attribution-NonCommercial License, which permits use, distribution and reproduction in any medium, provided the original work is properly cited and is not used for commercial purposes.

© 2024 Shell Global Solutions International B.V. *Geophysical Prospecting* published by John Wiley & Sons Ltd on behalf of European Association of Geoscientists & Engineers.



to ray tracing or one-way wave-equation approximations in mildly complex subsurface models and to ‘two-way’ constant- or variable-density acoustic or elastic propagators, typically implemented by finite-difference or finite-element methods. The ‘two-way’ approach can handle multi-pathing. To avoid multiple reflections with the latter, a reflection-free background model is often used. The subsurface model is split into a smooth component for the background and a rough component, the difference between the original and smoothed model, representing the reflectors. This distinction is called scale separation by Claerbout (1985). The Born approximation of the wave equation can model the primary reflections (Mulder & Plessix, 2004; Østmo et al., 2002; Tarantola, 1984). Fitting these to the observed data provides a subsurface migration image. This approach was originally called linearized inversion (Beylkin & Burridge, 1990; Plessix & Mulder, 2004; Tarantola, 1984) to distinguish it from the highly nonlinear FWI problem, but nowadays it is often referred to as least-squares reversed-time migration (Nemeth et al., 1999). The subsurface model is split into a background model that contains the smooth components of the velocity model and reflectors, which are perturbations of the model. In the Born approximation, the wave interaction between reflectors is ignored, resulting in an inverse problem that is linear in the perturbation parameters.

That leaves the nonlinear problem of finding an accurate background velocity model. If that model is incorrect, events do not focus after migration. The redundancy in the data offers a means to improve the model. Migration velocity analysis refers to methods that require the reflector positions to be independent of the redundant coordinates over which the data are summed. The simplest example is the normal move-out correction, useful in horizontally layered media. If the reflector depth increases with source–receiver offset, the velocity should be decreased, and if its depth decreases, the effective velocity is too high. If travel times are obtained with ray tracing, the depth should be constant for different reflection angles. Any residual move-out suggests a velocity update along the ray, which can be accounted for by the perturbed ray traveltimes equation (e.g., Mulder, 2006).

In the context of the ‘two-way’ wave equation, reflection angles are not readily available and other types of redundant coordinates may be considered. Horizontal shot coordinates (Kern & Symes, 1994) or offsets (Mulder & ten Kroode, 2002) are the first that come to mind, but in complex models the associated waves may illuminate different parts of the subsurface, making a comparison for constant reflector positions with nearby shot positions or offsets complicated. The shot and receiver position can be replaced by other redundant coordinates, similar to reflection angles in ray tracing. An example is the use of subsurface offsets (de Bruin et al., 1990; Mulder, 2008; Rickett & Sava, 2002; Shen & Symes, 2008; Symes, 2008), which can be interpreted as action at a distance. An incoming wave moves instantaneously from the point where

it hits the reflector to another point where it leaves and travels back to the receivers. A time-shift extension (Audebert and Diet, 2005; Chauris & Benjema, 2010; de Vries & Berkhout, 1984; Faye & Jeannot, 1986; Higginbotham et al., 2008; MacKay & Abma, 1992; Nemeth, 1996; Sava & Fomel, 2006; Symes, 2008; Yang & Sava, 2011) lets the wave jump backward or forward in time at the reflector. Note that these operations can be applied uniformly throughout the subsurface to avoid the explicit identification of reflectors. Other extensions involve shifts in source (Huang et al., 2019; Symes, 2023; Zhang & Gao, 2008) or receiver positions or time shifts in the data (Luo & Schuster, 1991; van Leeuwen & Mulder, 2008; van Leeuwen & Herrmann, 2013; Warner & Guasch, 2016).

The best velocity provides optimal focusing at zero shift. The underlying nonlinear optimization problem is often easier to solve than FWI and suffers less from local minima, in particular when the data lack sufficiently low frequencies. Remnant multiples in the preprocessed data, however, can cause problems (Barnier et al., 2023; Mulder & van Leeuwen, 2008; Mulder, 2014; Weibull & Arntsen, 2013). Nevertheless, the method may help to provide an initial model for FWI.

As already mentioned, this paper does not target velocity updating but uses the time-shift extended migration image to estimate the depth error of a velocity model constructed from seismic data. First, an explicit expression for the depth error in a constant velocity model for a reflector with a constant dip angle is derived using the stationary-phase approximation. The depth error depends on the apparent reflector dip and the position and time shift of the focusing point. As the effective velocity from the source to the reflector and on towards the receiver does not appear explicitly, the result may be generalized to the variable-velocity case, following the reasoning of Higginbotham et al. (2008), although it remains an approximation. As a proof of principle, the method is used to estimate the depth errors of a partially converged velocity model obtained from two-dimensional synthetic Born data for a salt diapir model, using an existing implementation of the focusing method (Mulder, 2008, 2014) with time shifts instead of subsurface offsets.

STATIONARY-PHASE METHOD FOR A CONSTANT VELOCITY

The method of stationary phase (van der Corput, 1935; Erdélyi, 1956) provides an approximation to an integral of an oscillatory function in the high-frequency limit for ω :

$$\int_{\Omega} d\mathbf{x} f(\mathbf{x}) e^{i\omega\psi(\mathbf{x})} \simeq \left(\frac{(2\pi)^d}{\omega^d |\det(\mathbf{H}_0)|} \right)^{1/2} f(\mathbf{x}_0) e^{i\omega\psi(\mathbf{x}_0) + i\frac{\pi}{4}\sigma(\mathbf{H}_0)}. \quad (1)$$

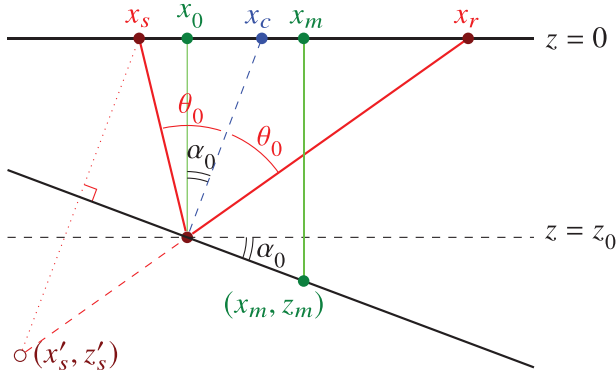


FIGURE 1 Reflector with dip angle α_0 , source at $(x_s, 0)$, receiver at $(x_r, 0)$, midpoint $(x_m, 0)$, half offset $h = (x_r - x_s)/2$, mirrored source at (x'_s, z'_s) , reflection point (x_0, z_0) . Half the reflection angle is θ_0 .

The gradient of the phase $\psi(\mathbf{x})$ vanishes at $\mathbf{x} = \mathbf{x}_0$, in the interior of the domain Ω in d dimensions. Its Hessian $\mathbf{H}_0 = \mathbf{H}(\psi(\mathbf{x}_0))$ is assumed to have a non-zero determinant $\det(\mathbf{H}_0)$ with a signature $\sigma(\mathbf{H}_0)$, defined as the number of positive minus the number of negative eigenvalues. In the case of multiple roots for $\psi(\mathbf{x}) = 0$, the contributions at the roots should be summed.

Travel time for a dipped reflector

Liu and Bleistein (1995) derived the travel time for a dipped reflector with the stationary-phase method. Their approach is repeated here to define the notation, also illustrated in Figure 1.

Consider a reflector with dip angle α_0 in a two-dimensional homogeneous model with constant velocity v_0 . A straight-line reflector is defined by a depth $z(x) = z_a + (x - x_a) \tan \alpha_0$ for a reference point (x_a, z_a) . The source is located at (x_s, z_s) and the receiver at (x_r, z_r) , with $z_s = z_r = 0$ at the surface. The half-offset is $h = (x_r - x_s)/2$, and the midpoint is $x_m = (x_r + x_s)/2$. Assume $h \geq 0$ and $0 < \alpha_0 < \pi/2$. The travel time to a subsurface point (x, z) is $\tau = \tau_s + \tau_r$, with $\tau_{s,r} = v_0^{-1} \sqrt{z^2 + (x - x_{s,r})^2}$. The reflection point on the dipped reflector in the high-frequency limit can be found by requiring $\partial\tau/\partial x = 0$, using $z(x)$ on the reflector. The corresponding equation is

$$v_0 \frac{\partial\tau}{\partial x} = \frac{x - x_m + h + z \tan \alpha_0}{\sqrt{z^2 + (x - x_m + h)^2}} + \frac{x - x_m - h + z \tan \alpha_0}{\sqrt{z^2 + (x - x_m - h)^2}} = 0, \quad (2)$$

where $z(x) = z_a + (x - x_a) \tan \alpha_0$. To solve the equation, it is more convenient to replace x by z , assuming non-zero dip, $\alpha_0 \neq 0$, and positive depth, $z > 0$. If $z_m = z_a + (x_m - x_a) \tan \alpha_0$ is the depth of the point on the reflector vertically below the midpoint x_m , then Equation (2), after multiplication

by $\cot \alpha_0$, can be written as

$$\begin{aligned} & \frac{z + [(z - z_m) \cot(\alpha_0) + h] \cot \alpha_0}{\sqrt{z^2 + [(z - z_m) \cot(\alpha_0) + h]^2}} + \\ & \frac{z + [(z - z_m) \cot(\alpha_0) - h] \cot \alpha_0}{\sqrt{z^2 + [(z - z_m) \cot(\alpha_0) - h]^2}} = 0. \end{aligned} \quad (3)$$

The solution for the scatter point (x_0, z_0) that has $z_0 > 0$ is

$$x_0 - x_m = -\sin(\alpha_0) \cos(\alpha_0) (z_m^2 + h^2) / z_m, \quad (4a)$$

$$z_0 - z_m = (x_0 - x_m) \tan \alpha_0 = -\sin^2(\alpha_0) (z_m^2 + h^2) / z_m, \quad (4b)$$

if $z_m > h \tan \alpha_0$, that is, if the reflector does not cut the surface at a point between the source and receiver. The distance of the scatter point on the reflector to the source becomes

$$d_{0,s} = [1 - (h/z_m) \tan \alpha_0] \cos(\alpha_0) \sqrt{h^2 + z_m^2}, \quad (5a)$$

and to the receiver

$$d_{0,r} = [1 + (h/z_m) \tan \alpha_0] \cos(\alpha_0) \sqrt{h^2 + z_m^2}. \quad (5b)$$

From the expressions for the scattering point, it follows that half the scattering angle θ_0 obeys $\tan \theta_0 = h/z_m$. Then, under the condition $\tan \alpha_0 < \cot \theta_0$,

$$d_{0,s} = z_0 / \cos(\theta_0 - \alpha_0), \quad d_{0,r} = z_0 / \cos(\theta_0 + \alpha_0), \quad (6)$$

identical to Equation (14) of Liu and Bleistein (1995). Also,

$$x_0 - x_m = -h \frac{\sin \alpha_0 \cos \alpha_0}{\sin \theta_0 \cos \theta_0}, \quad (7a)$$

$$z_0 - z_m = -h \frac{\sin^2 \alpha_0}{\sin \theta_0 \cos \theta_0}. \quad (7b)$$

The two-way travel time becomes $\tau = 2v_0^{-1} \cos(\alpha_0) \sqrt{h^2 + z_m^2}$ for $z_m > h \tan \alpha_0$.

Geometrical arguments and Snell's law produce the same result. The mirror source in Figure 1 at (x'_s, z'_s) is defined by a line from $(x_s, 0)$ to (x'_s, z'_s) that should be orthogonal to the reflector and have a point halfway on the reflector:

$$(x'_s - x_s) / (z'_s - 0) = -\tan \alpha_0, \quad (8a)$$

$$\frac{1}{2}(z'_s + 0) = z_a + \left[\frac{1}{2}(x_s + x'_s) - x_a \right] \tan \alpha_0. \quad (8b)$$

The solution is

$$x'_s = x_a + (x_s - x_a) \cos(2\alpha_0) - z_a \sin(2\alpha_0), \quad (9a)$$

$$z'_s = 2[z_a + (x_s - x_a) \tan \alpha_0] \cos^2 \alpha_0, \quad (9b)$$

providing a distance $d_{s',r} = v_0 \tau = 2 \cos(\alpha_0) \sqrt{h^2 + z_m^2}$ between (x'_s, z'_s) and $(x_r, 0)$. The normal to the reflector at the point of specular reflection intersects the surface at $x_c = x_0 + z_0 \tan \alpha_0 = x_m - (h^2/z_m) \tan \alpha_0 = x_m - h \tan(\alpha_0) \tan(\theta_0)$.

Time-shift imaging

The extended migration image in a model with velocity v of data obtained with velocity v_0 and an additional time shift Δt is given by

$$R(x, z; \Delta t) = \int_{h_{\min}}^{h_{\max}} \int_{-\infty}^{\infty} dx_m A(x_s, z_s; x, z) A(x_r, z_r; x, z) e^{i\omega\psi}, \quad (10)$$

where the phase $\psi = \tau(h, x_m; v_0) - \tau_s(x, z; v) - \tau_r(x, z; v) - 2\Delta t$. The amplitudes $A(x_{s,r}, z_{s,r}; x, z)$ from source or receiver to depth point (x, z) are not important in what follows. For now, an infinite offset range is assumed.

Stationarity involves the equations $\psi = 0$, $\partial\psi/\partial h = 0$ and $\partial\psi/\partial x_m = 0$ for Δt , h and x_m . The first equation directly provides the stationary time shift Δt . The remaining two are

$$\frac{2\beta h \cos \alpha_0}{\sqrt{h^2 + z_m^2}} = \frac{h - x_1}{\sqrt{(h - x_1)^2 + z^2}} + \frac{h + x_1}{\sqrt{(h + x_1)^2 + z^2}}, \quad (11a)$$

$$\frac{2\beta z_m \sin \alpha_0}{\sqrt{h^2 + z_m^2}} = \frac{h - x_1}{\sqrt{(h - x_1)^2 + z^2}} - \frac{h + x_1}{\sqrt{(h + x_1)^2 + z^2}}, \quad (11b)$$

where $\beta = v/v_0$ and $x_1 = x - x_m$, with z_m depending on x_m or x_1 .

There are two solutions.

The *first* is given by $h = 0$ and $x_1 = x - x_m = -z \tan \alpha$. Here, α is defined by $\sin \alpha = \beta \sin \alpha_0$ and equals the apparent dip angle of the reconstructed reflector after migration, as long as $|\sin \alpha_0| < 1/\beta$ for $\beta = v/v_0$. The time shift Δt at the reflection point (x, z) for the first solution follows from $\psi = 0$:

$$\Delta t(x, z) = \frac{\cos \alpha}{v} (z_{\text{mig}} - z), \quad (12)$$

where

$$z_{\text{mig}} = z_b + (x - x_a) \tan \alpha, \quad z_b = z_a \frac{\tan \alpha}{\tan \alpha_0}, \quad (13)$$

is the depth of the reflector after migration at zero time shift. This shows that the apparent dip angle is indeed α and that the reference point has moved from z_a to z_b . In the correct model, $\beta = v/v_0 = 1$, $\alpha = \alpha_0$, and the stationary time shift $\Delta t = 0$.

Before going to the second solution, the Hessian is examined.

The amplitude along the straight line $\Delta t(z)$ at fixed x , and $h = 0$ is inversely proportional to the square root of the absolute value of the determinant of the Hessian with respect to h and x_m at the stationary point. In this case,

$$\mathbf{H}_0 = -\frac{2\cos^3 \alpha}{vz} \text{diag} \left\{ 1 - \frac{z \tan \alpha}{z_c \tan \alpha_0 \cos^2 \alpha}, 1 \right\} \quad (14)$$

with

$$z_c = z_a + (x - x_a) \tan \alpha_0 + z \tan \alpha \tan \alpha_0. \quad (15)$$

Note that $z_c > 0$, because the true reflector depth $z_a + (x - x_a) \tan \alpha_0$ is assumed to be positive, only positive depths z are considered, α and α_0 have the same sign because $\sin \alpha = \beta \sin \alpha_0$ with $\beta = v/v_0 > 0$ and it is assumed that $0 < \alpha_0 < \pi/2$, $0 < \alpha < \pi/2$ and $0 < \beta \sin \alpha_0 < 1$.

The second diagonal value of the Hessian is negative. For a given x , the first diagonal value changes sign at the point defined by z_{peak} and Δt_{peak} , where the determinant of the Hessian becomes zero:

$$z_{\text{peak}} = \frac{z_{\text{mig}}}{\tan^2 \alpha [1/(\tan \alpha_0 \cos \alpha)^2 - 1]}, \quad (16a)$$

and

$$\Delta t_{\text{peak}} = \frac{\cos \alpha}{v} (z_{\text{mig}} - z_{\text{peak}}). \quad (16b)$$

At this point, the amplitude in Equation (1) appears to become infinite. To obtain a finite result, higher-order non-zero terms of the expansion into h and x_m should be included in the stationary phase method, but that is beyond the scope of this paper.

In the correct model with $\beta = 1$, $z_{\text{peak}} = z_{\text{mig}} = z_0$ and $\Delta t_{\text{peak}} = 0$.

The signature $\sigma(\mathbf{H}_0) = -2$ if $1 - (z \tan \alpha)/(z_c \tan \alpha_0 \cos^2 \alpha) > 0$, which can be simplified to $(z - z_{\text{peak}})(\cos^2 \alpha - \cot^2 \alpha_0) > 0$. If the expression is negative, $\sigma(\mathbf{H}_0) = 0$. This implies that the amplitudes for $z < z_{\text{peak}}$ and $z > z_{\text{peak}}$ have a 90° phase difference.

The *second* solution of the stationary-phase equations with $h \neq 0$ can be obtained by solving the stationary-phase equations (11) in terms of $z(x, \theta_0)$, $x_m(x, \theta_0)$ instead of $x_m(x, z)$ and $h(x, z)$. Define

$$\xi_{\pm} = (x - x_m) \pm h = (x - x_m) \pm z_m \tan \theta_0. \quad (17)$$

The system (11) becomes

$$2\beta \cos(\alpha_0) \sin(\theta_0) = \frac{\xi_+}{\sqrt{\xi_+^2 + z^2}} - \frac{\xi_-}{\sqrt{\xi_-^2 + z^2}}, \quad (18a)$$

$$2\beta \sin(\alpha_0) \cos(\theta_0) = -\frac{\xi_+}{\sqrt{\xi_+^2 + z^2}} - \frac{\xi_-}{\sqrt{\xi_-^2 + z^2}}. \quad (18b)$$

After taking the sum and difference of these equations, the system simplifies to

$$\xi_+ = \beta \sin(\theta_0 - \alpha_0) \sqrt{\xi_+^2 + z^2}, \quad (19a)$$

$$\xi_- = -\beta \sin(\theta_0 + \alpha_0) \sqrt{\xi_-^2 + z^2}, \quad (19b)$$

which can be reduced to

$$z = \xi_+/q_- = -\xi_-/q_+, \quad q_{\pm} = \tan \theta_{\pm}, \quad (20)$$

with

$$\sin \theta_{\pm} = \beta \sin(\theta_0 \pm \alpha_0). \quad (21)$$

Assuming a dip angle $\alpha_0 \geq 0$ and scattering angle $\theta_0 \geq 0$, as in Figure 1, the last expression implies

$$0 \leq \theta_0 \leq \arcsin(\min(1, 1/\beta)) - \alpha_0. \quad (22)$$

Solving x_m and z from $\xi_+ + \xi_- = 2x_m$ and $\xi_+ - \xi_- = 2h$ with $z_m = x_a + (x_m - x_a) \tan \alpha_0$ and $h = z_m \tan \theta_0$ produces

$$x - x_m = \frac{[z_a + (x - x_a) \tan \alpha_0](q_+ - q_-) \cos(\alpha_0) \sin(\theta_0)}{q_+ \cos(\theta_0 - \alpha_0) + q_- \cos(\theta_0 + \alpha_0)}, \quad (23)$$

from which z_m , h and

$$z = \frac{2h}{q_+ + q_-} \quad (24)$$

are found. Finally, the condition $\psi = 0$ provides

$$\Delta t = \frac{z_m}{v} \left[\beta \frac{\cos(\alpha_0)}{\cos(\theta_0)} - \tan(\theta_0) \frac{\cos(\theta_+) + \cos(\theta_-)}{\sin(\theta_+ + \theta_-)} \right]. \quad (25)$$

In the limit for $\theta_0 \rightarrow 0$, $z = z_{\text{peak}}$ and $\Delta t = \Delta t_{\text{peak}}$, showing that the starting point of the second solution coincides with the point where the Hessian vanishes.

For zero dip angle $\alpha_0 = 0$, the reflector depth is $z_{\text{mig}} = z_b = \beta z_a$ and the first solution has $h = 0$ and $\Delta t = v^{-1}(\beta z_a - z)$. The second has $x_m = x$, $h = [(z_a^2 - \beta^2 z^2)/(\beta^2 - 1)]^{1/2}$ and $\Delta t = v^{-1}(\beta^2 - 1)[(z_a^2 - z^2)/(\beta^2 - 1)]^{1/2}$ (Sava & Fomel, 2006). In addition, $z_{\text{peak}} = z_a/\beta$ and $z_{\text{mig}} = z_a\beta$, implying $z_a = (z_{\text{mig}} z_{\text{peak}})^{1/2}$ (Faye & Jeannot, 1986).

Depth error

The apparent dip angle at $h = 0$ and $\Delta t = 0$ can be estimated from $\partial z/\partial \Delta t = -v/\cos \alpha$ or $\partial z/\partial x = \tan \alpha$, where the second expression avoids a sign ambiguity. With that and the migration depth z_{mig} at zero time shift, z_{peak} can be located along the line $\Delta t = v^{-1}(z_{\text{mig}} - z) \cos \alpha$. The depth error follows from

$$z_{\text{mig}} - z_0 = z_{\text{mig}} \left(1 - \frac{\tan \alpha_0}{\tan \alpha} \right), \quad (26)$$

where

$$\frac{\tan \alpha_0}{\tan \alpha} = \left[1 + \left(\frac{z_{\text{mig}}}{z_{\text{peak}}} - 1 \right) \cos^2 \alpha \right]^{-1/2}. \quad (27)$$

For small dip, $z_{\text{mig}} - z_0 \simeq z_{\text{mig}}(1 - \sqrt{z_{\text{peak}}/z_{\text{mig}}})$ (Faye & Jeannot, 1986).

The time-shifted migration image in an arbitrary velocity model is defined as

$$R(x, z; \Delta t) = \sum_s \sum_{r(s)} \int_{\Omega} dt p_s(\mathbf{x}, t + \Delta t/2) q_{r(s)}(\mathbf{x}, t - \Delta t/2), \quad (28)$$

with $p_s(\mathbf{x}, t)$ the forward wavefield as function of position $\mathbf{x} \in \Omega$ and time t for a source enumerated by s and $q_{r(s)}(\mathbf{x}, t)$ the reverse-time wavefield for the receivers labelled by $r(s)$ for source s . Note the definition has a sign for the time shift Δt that is the opposite of what is chosen in several other publications.

To estimate z_{peak} at a given x and $z = z_{\text{mig}}$, determine the apparent dip angle α from $R(x, z; \Delta t = 0)$, rotate the extended image by $\arctan(-v(x, z)/\cos \alpha)$, track along the nearly horizontal event to find the peak amplitude and its position and then rotate back to find z_{peak} .

If the velocity is not constant, the straight-line solution becomes curved (Duvencq, 2021). The curve can be constructed by solving the ordinary differential equation $d\zeta/d\Delta t = v(\zeta)/\cos \alpha(\zeta)$ for $\zeta(x, z; \Delta t)$ at given x and z , with initial condition $\zeta(x, z; \Delta t = 0) = z$. The integration is performed separately in the positive and negative direction of Δt . Interpolation in z then provides $R(x, \zeta; \Delta t)$, and the peak values $\Delta t_{\text{peak}}(x, \zeta)$ can be determined along horizontal lines, at constant ζ . The result is assigned to $\Delta t_{\text{peak}}(x, z)$, leading to $z_{\text{peak}}(x, z) = \zeta(x, z; \Delta t_{\text{peak}})$.

COMPARISON TO FINITE-FREQUENCY RESULTS

To illustrate the result, Born scattering data were generated with a two-dimensional frequency-domain finite-difference code (Mulder & Plessix, 2002) for a velocity model with

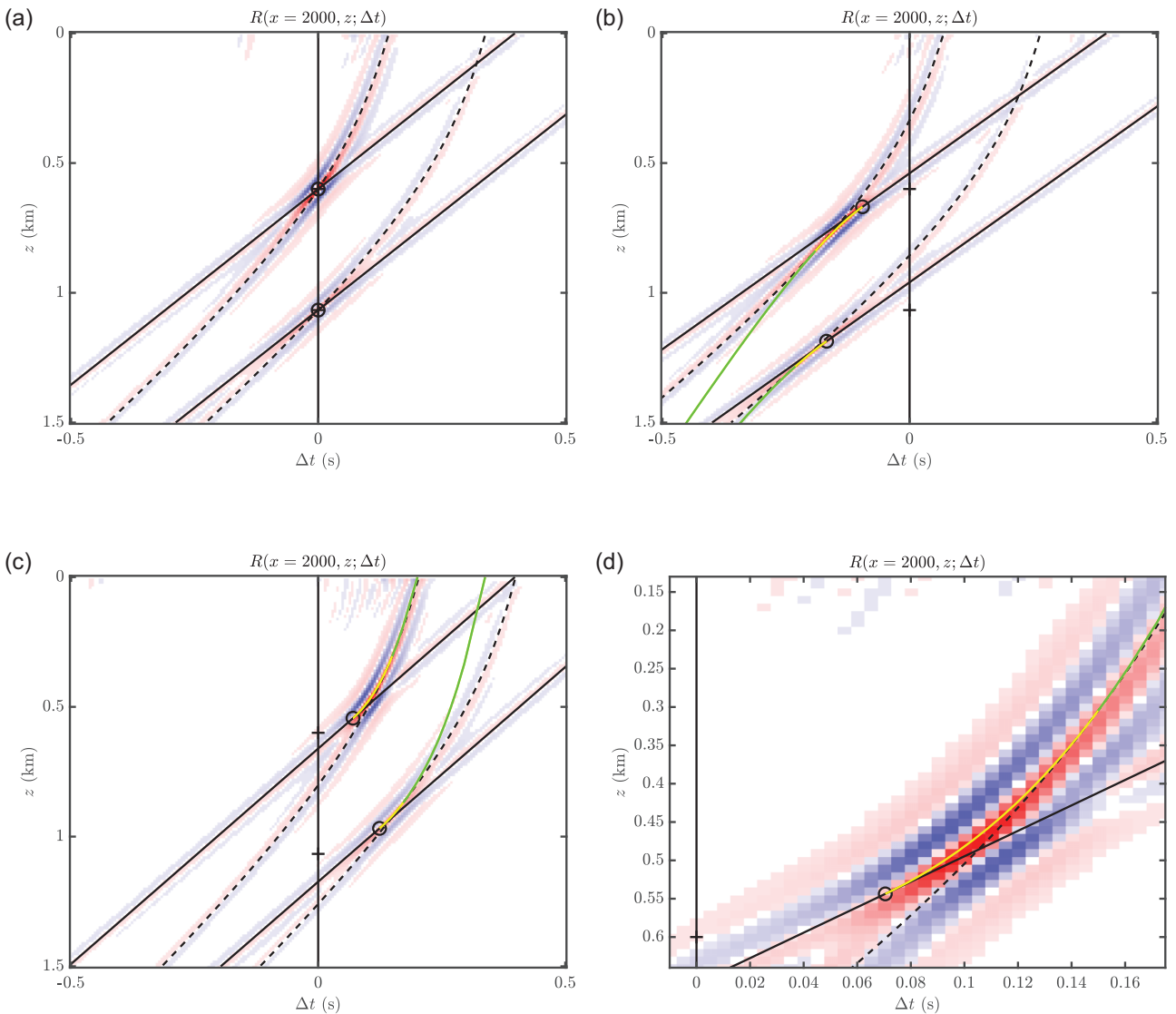


FIGURE 2 (a) Extended image at fixed $x = 2000$ m and a function of time shift Δt and depth z for the true velocity. The drawn line represents the first solution of the stationary-phase equations, and the circle denotes the expected position of the maximum amplitude. The dashed lines correspond to the maximum offset. (b) As (a) but for too low a velocity of 1350 m/s. The drawn yellow curves represent the second solution, with the green part corresponding to offsets larger than the maximum offset in the data. The true depth of the reflector is marked by a small horizontal line segment at zero time shift. (c) As (a) but for too high a velocity of 1650 m/s. (d) Detail of (c).

$v_0 = 1500$ m/s and two reflectors. The first had a depth of 400 m at $x = 0$ and 700 m at $x = 3000$ m, the second a depth of 1200 m at $x = 0$ and 1000 m at $x = 3000$ m, resulting in dip angles of 5.71 and -3.81 degrees. Shots at zero depth ranged from $x_s = 0$ to 3000 m with a 50-m spacing and a 15-Hz Ricker wavelet. Receivers had offsets $h = x_r - x_s$ from 0 to 2000 m at a 25-m interval in a marine-type acquisition.

Figure 2a shows the extended image in the correct velocity model, obtained with the same finite-difference code. Figure 2b corresponds to a velocity that is 10% smaller and Figure 2c,d for 10% larger.

The straight-line solutions are drawn as black lines. The amplitude along these lines changes its phase by 90° relative

to the peak location, marked by an open circle, as predicted by the stationary-phase analysis. This is only visible at some distance because of interference with the second solution.

With a finite acquisition, the endpoint in the stationary-phase integral has to be included. Given a maximum half-offset h_{\max} and a time shift Δt following from $\psi = 0$, this leaves the equation $\partial\psi/\partial x_m = 0$. Solving for x_m leads to Δt as a function of z at fixed x , shown with a dashed black line in Figure 2. In the absence of a proper acquisition taper, the second solution at zero time shift shows up as an additional apparent reflector interface in the migration image.

The second solution is drawn in yellow for offsets $h \leq h_{\max}$ and in green for $h > h_{\max}$. It starts at the peak location and

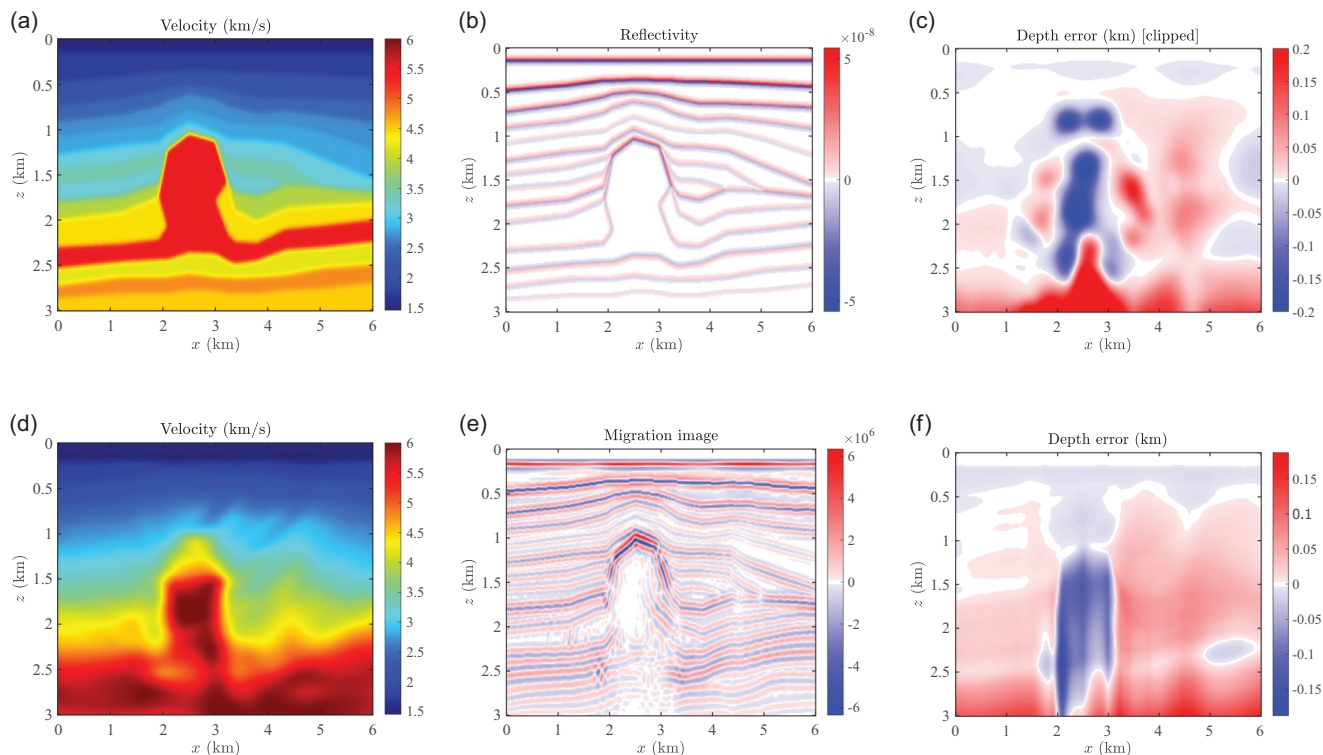


FIGURE 3 Velocity model (a) and reflectivity (b) for the true model and the estimated error (c), clipped at ± 200 m, for the recovered model (d), the related depth-weighted migration image (e), and a crude estimate of the depth error obtained by comparing the recovered and exact velocity model (f).

curves towards more negative Δt and larger depths z if the velocity is too small, and in the opposite direction of the velocity is too large.

In the finite-frequency case and with an incorrect velocity, the peak value along the straight-line solution does not occur at the predicted location. This is mainly caused by the interference with the curved second solution that starts at the predicted peak location and, to a lesser extent, with the curve for the maximum offset. The net effect will be an over-estimate of the depth error.

AN APPLICATION

To examine the potential use of the derived depth-error estimate, the two-dimensional velocity model of Figure 3a, taken from Mulder (2001), was considered. Born scattering data for the reflectivity shown in Figure 3b were generated for a land-type acquisition with shots between -950 and 6950 m at a 50 -m interval with a 15 -Hz Ricker wavelet and receivers between -962.5 and 6962.5 m at a 25 -m interval.

Figure 3d displays a reconstructed velocity model represented by cubic B-splines and obtained by optimizing a focusing functional based on time-shift extended imaging, similar to Mulder (2008, 2014) but with subsurface shifts replaced by time shifts. Note that this method does not explic-

itly include depth errors but only tries to move energy in the image to zero shift. The shown model corresponds to an intermediate result, starting from the best linear-in-depth velocity with a given surface velocity. Figure 3e shows the corresponding depth-weighted migration image. The data were differentiated in time to change the zero crossing of the reflectivity in Figure 3b at the position of a reflector interface into a peak in Figure 3e. Figure 3c displays the depth errors, expected to be over-estimated and affected by the cubic-spline representation of the background model. The impact of the salt diapir is obvious, as is the increase in error with depth. For comparison, Figure 3f shows a crude estimate of the depth error obtained from $\int_0^z dz' [1 - v_0(x, z')/v(x, z')]$, which ignores strong lateral variations. This shows that, although the focusing of energy in an extended image can be fairly effective for the construction of an initial velocity model from primaries-only data, this appears to be less so for the more delicate depth-error estimation outlined here, at least for its present implementation, although the overall trend is more or less correct.

CONCLUSIONS

The stationary-phase method applied to migration with a time-shift extension in a 2-D constant-velocity model with a



dipped reflector produces two solutions, one a straight line, and the other is a curve, similar to the case of a horizontal reflector (Sava & Fomel, 2006). The depth error follows from the apparent reflector dip and depth as well as the depth of the amplitude peak along the first solution in the time-shift extended image, where the second solution meets. The method was applied to estimate the depth errors in a 2-D synthetic example with a salt diapir.

ACKNOWLEDGEMENTS

The author is indebted to Eric Duveneck and Boris Kuvshinov for their helpful comments and to Koos de Vos for pointing out the phase change behaviour. A preliminary version was presented at the EAGE 2023 Annual Meeting (Mulder, 2023).

DATA AVAILABILITY STATEMENT

Data sharing is not applicable to this article as no new data were created or analysed in this study. However, if the computational results shown in the Figures are considered as new data, then the author elects not to share those.

ORCID

W. A. Mulder  <https://orcid.org/0000-0001-7020-9297>

REFERENCES

- Audebert, F. & Diet, J.P. (2005) Migrated focus panels: Focusing analysis reconciled with prestack depth migration. In: *SEG Technical Program Expanded Abstracts 1993*. Houston, TX: Society of Exploration Geophysicists, pp. 961–964. <https://doi.org/10.1190/1.1822668>
- Backus, G. & Gilbert, F. (1970) Uniqueness in the inversion of inaccurate gross Earth data. *Philosophical Transactions of the Royal Society of London. Series A, Mathematical and Physical Sciences*, 266(1173), 123–192. <https://doi.org/10.1098/rsta.1970.0005>
- Barnier, G., Biondi, E., Clapp, R.G. & Biondi, B. (2023) Full-waveform inversion by model extension: practical applications. *Geophysics*, 88(5), R609–R643. <https://doi.org/10.1190/GEO2022-0382.1>
- Beylkin, G. & Burridge, R. (1990) Linearized inverse scattering problems in acoustics and elasticity. *Wave Motion*, 12(1), 15–52. [https://doi.org/10.1016/0165-2125\(90\)90017-X](https://doi.org/10.1016/0165-2125(90)90017-X)
- Chauris, H. & Benjema, M. (2010) Seismic wave-equation demigration/migration. *Geophysics*, 75(3), S111–S119. <https://doi.org/10.1190/1.3380705>
- Claerbout, J. (1985) *Imaging the Earth's Interior*, Oxford, UK: Blackwell Science Inc.
- de Bruin, C.G.M., Wapenaar, C.P.A. & Berkhout, A.J. (1990) Angle-dependent reflectivity by means of prestack migration. *Geophysics*, 55(9), 1223–1234. <https://doi.org/10.1190/1.1442938>
- de Vries, D. & Berkhout, A.J. (1984) Influence of velocity errors on the focusing aspects of migration. *Geophysical Prospecting*, 32, 629–648. <https://doi.org/10.1111/j.1365-2478.1984.tb01710.x>
- Duveneck, E. (2021) Angle gathers from time-shift extended least-squares reverse-time migration. In: *Conference Proceedings of the 82nd EAGE Annual Conference & Exhibition*, Houten, the Netherlands: European Association of Geoscientists & Engineers, pp. 1–5. <https://doi.org/10.3997/2214-4609.202113232>
- Erdélyi, A. (1956) *Asymptotic expansions*. New York: Dover.
- Faye, J.-P. & Jeannot, J.-P. (1986) Prestack migration velocities from focusing depth analysis. In: *SEG Technical Program Expanded Abstracts 1986*. Houston, TX: Society of Exploration Geophysicists, pp. 438–440. <https://doi.org/10.1190/1.1893053>
- Higginbotham, J.H., Brown, M.P. & Clapp, R.G. (2008) Wave equation migration velocity focusing analysis, in *SEG Technical Program Expanded Abstracts 2008*. Houston, TX: Society of Exploration Geophysicists, pp. 3083–3087. <https://doi.org/10.1190/1.3063985>
- Huang, G., Nammour, R., Symes, W.W. & Dolia, M. (2019) Waveform inversion via source extension. In: *SEG Technical Program Expanded Abstracts 2019*. Houston, TX: Society of Exploration Geophysicists, pp. 4761–4766. <https://doi.org/10.1190/segam2019-3216338.1>
- Kern, M. & Symes, W.W. (1994) Inversion of reflection seismograms by differential semblance analysis: algorithm structure and synthetic examples. *Geophysical Prospecting*, 42(6), 565–614. <https://doi.org/10.1111/j.1365-2478.1994.tb00231.x>
- Liu, Z. & Bleistein, N. (1995) Migration velocity analysis: Theory and an iterative algorithm. *Geophysics*, 60(1), 142–153. <https://doi.org/10.1190/1.1443741>
- Luo, Y. & Schuster, G.T. (1991) Wave-equation travelt ime inversion. *Geophysics*, 56(5), 645–653. <https://doi.org/10.1190/1.1443081>
- MacKay, S. & Abma, R. (1992) Imaging and velocity estimation with depth-focusing analysis. *Geophysics*, 57(12), 1608–1622. <https://doi.org/10.1190/1.1443228>
- Mulder, W.A. (2001) Higher-order mass-lumped finite elements for the wave equation. *Journal of Computational Acoustics*, 9(2), 671–680. <https://doi.org/10.1142/S0218396X0100067X>
- Mulder, W.A. (2006) The perturbed travelt ime equation and the adjoint-states gradient of the travelt ime error. *Geophysical Journal International*, 167(2), 679–683. <https://doi.org/10.1111/j.1365-246X.2006.02932.x>
- Mulder, W.A. (2008) Automatic velocity analysis with the two-way wave equation. In: *Conference Proceedings of the 70th EAGE Conference and Exhibition incorporating SPE EUROPEC 2008*. Houten, the Netherlands: European Association of Geoscientists & Engineers, pp. 1–5. <https://doi.org/10.3997/2214-4609.20147941>
- Mulder, W.A. (2014) Subsurface offset behaviour in velocity analysis with extended reflectivity images. *Geophysical Prospecting*, 62(1), 17–33. <https://doi.org/10.1111/1365-2478.12073>
- Mulder, W.A. (2023) Time-shift extended imaging for estimating depth errors. In: *Conference Proceedings of the 84th EAGE Annual Conference & Exhibition*. Houten, the Netherlands: European Association of Geoscientists & Engineers, pp. 1–5. <https://doi.org/10.3997/2214-4609.202310690>
- Mulder, W.A. & Kuvshinov, B.N. (2023) Estimating large-scale uncertainty in the context of full-waveform inversion. In: *Conference Proceedings of the 84th EAGE Annual Conference & Exhibition*. Houten, the Netherlands: European Association of Geoscientists & Engineers, vol. 2023, pp. 1–5. <https://doi.org/10.3997/2214-4609.202310304>
- Mulder, W.A. & Plessix, R.-É. (2002) Time-versus frequency-domain modelling of seismic wave propagation. In: *Conference Proceedings of the 64th EAGE Conference & Exhibition*. Houten, the Netherlands: European Association of Geoscientists & Engineers, pp. 1–5. <https://doi.org/10.3997/2214-4609-pdb.5.E015>
- Mulder, W.A. & Plessix, R.-É. (2004) A comparison between one-way and two-way wave-equation migration. *Geophysics*, 69(6), 1491–1504. <https://doi.org/10.1190/1.1836822>



- Mulder, W.A. & ten Kroode, A. P.E. (2002) Automatic velocity analysis by differential semblance optimization. *Geophysics*, 67(4), 1184–1191. <https://doi.org/10.1190/1.1500380>
- Mulder, W.A. & van Leeuwen, T. (2008) Automatic migration velocity analysis and multiples. In: *SEG Technical Program Expanded Abstracts 2008*. Houston, TX: Society of Exploration Geophysicists, pp. 3128–3132. <https://doi.org/10.1190/1.3063996>
- Nemeth, T. (1996) Relating depth-focusing analysis to migration velocity analysis. In: *SEG Technical Program Expanded Abstracts 1996*. Houston, TX: Society of Exploration Geophysicists, pp. 463–466. <https://doi.org/10.1190/1.1826675>
- Nemeth, T., Wu, C. & Schuster, G.T. (1999) Least-squares migration of incomplete reflection data. *Geophysics*, 64(1), 208–221. <https://doi.org/10.1190/1.1444517>
- Østmo, S., Mulder, W.A. & Plessix, R.-É. (2002) Finite-difference iterative migration by linearized waveform inversion in the frequency domain. In: *SEG Technical Program Expanded Abstracts 2002*. Houston, TX: Society of Exploration Geophysicists, pp. 1384–1387. <https://doi.org/10.1190/1.1816917>
- Plessix, R.-É. & Mulder, W.A. (2004) Frequency-domain finite-difference amplitude-preserving migration. *Geophysical Journal International*, 157(3), 975–987. <https://doi.org/10.1111/j.1365-246X.2004.02282.x>
- Rickett, J.E. (2003) Illumination-based normalization for wave-equation depth migration. *Geophysics*, 68(4), 1371–1379. <https://doi.org/10.1190/1.1598130>
- Rickett, J.E. & Sava, P.C. (2002) Offset and angle-domain common image-point gathers for shot-profile migration. *Geophysics*, 67(3), 883–889. <https://library.seg.org/doi/10.1190/1.1484531>
- Sava, P.C. & Fomel, S. (2006) Time-shift imaging condition in seismic migration. *Geophysics*, 71(6), S209–S217. <https://doi.org/10.1190/1.2338824>
- Schuster, G.T. (2017) *Seismic inversion*. Tulsa, OK: Society of Exploration Geophysicists. <https://doi.org/10.1190/1.9781560803423>
- Shen, P. & Symes, W.W. (2008) Automatic velocity analysis via shot profile migration. *Geophysics*, 73(5), VE49–VE59. <https://doi.org/10.1190/1.2972021>
- Symes, W.W. (2008) Migration velocity analysis and waveform inversion. *Geophysical Prospecting*, 56(6), 765–790. <https://doi.org/10.1111/j.1365-2478.2008.00698.x>
- Symes, W.W. (2023) Efficient computation of extended surface sources. *GEM - International Journal on Geomathematics*, 14, 3. <https://doi.org/10.1007/s13137-023-00213-0>
- Tarantola, A. (1984) Linearized inversion of seismic reflection data. *Geophysical Prospecting*, 32(6), 998–1015. <https://doi.org/10.1111/j.1365-2478.1984.tb00751.x>
- Tarantola, A. (2005) *Inverse problem theory and methods for model parameter estimation*. Philadelphia, PA: SIAM. <https://doi.org/10.1137/1.9780898717921>
- van der Corput, J.G. (1935) Zur Methode der stationären Phase. Erste Mitteilung Einfache Integrale. *Compositio Mathematica*, 1, 15–38.
- van Leeuwen, T. & Herrmann, F.J. (2013) Mitigating local minima in full-waveform inversion by expanding the search space. *Geophysical Journal International*, 195(1), 661–667. <https://doi.org/10.1093/gji/ggt258>
- van Leeuwen, T. & Mulder, W.A. (2008) Velocity analysis based on data correlation. *Geophysical Prospecting*, 56(6), 791–803. <https://doi.org/10.1111/j.1365-2478.2008.00704.x>
- Warner, M. & Guasch, L. (2016) Adaptive waveform inversion: Theory. *Geophysics*, 81(6), R429–R445. <https://doi.org/10.1190/geo2015-0387.1>
- Weibull, W.W. & Arntsen, B. (2013) Automatic velocity analysis with reverse-time migration. *Geophysics*, 78(4), S179–S192. <https://doi.org/10.1190/geo2012-0064.1>
- Yang, T. & Sava, P. (2011) Wave-equation migration velocity analysis with time-shift imaging. *Geophysical Prospecting*, 59(4), 635–650. <https://doi.org/10.1111/j.1365-2478.2011.00954.x>
- Zhang, Y. & Gao, F. (2008) Full waveform inversion based on reverse time propagation. In: *SEG Technical Program Expanded Abstracts 2008*. Houston, TX: Society of Exploration Geophysicists, pp. 1950–1955. <https://doi.org/10.1190/1.3059278>

How to cite this article: Mulder, W.A. (2024) Stationary-phase analysis of time-shift extended imaging in a constant-velocity model. *Geophysical Prospecting*, 1–9. <https://doi.org/10.1111/1365-2478.13496>